water

Article

Adsorption of Pb^{2+} by Activated Carbon Produced by Microwave-Assisted K_2CO_3 Activation of Date Palm Leaf Sheath Fibres

Saud S. Aloud [1], Bassim H. Hameed [2], Mohamad F. M. Yusop [3], Hattan A. Alharbi [4], John P. Giesy [5,6,7] and Khaled D. Alotaibi [1,*]

[1] Department of Soil Science, College of Food and Agriculture Sciences, King Saud University, P.O. Box 2460, Riyadh 11451, Saudi Arabia; saloud@ksu.edu.sa
[2] Department of Chemical Engineering, College of Engineering, Qatar University, Doha P.O. Box 2713, Qatar; b.hammadi@qu.edu.qa
[3] School of Chemical Engineering, Engineering Campus, Universiti Sains Malaysia, Nibong Tebal 14300, Penang, Malaysia; mfirdausyusop@yahoo.com
[4] Department of Plant Protection, College of Food and Agriculture Sciences, King Saud University, P.O. Box 2460, Riyadh 11451, Saudi Arabia; halharbii@ksu.edu.sa
[5] Department of Veterinary Biomedical Sciences and Toxicology Centre, University of Saskatchewan, Saskatoon, SK S7N 5B3, Canada; john.giesy@usask.ca
[6] Department of Integrative Biology and Integrative Toxicology Program, Michigan State University, East Lansing, MI 48824, USA
[7] Department of Environmental Sciences, Baylor University, Waco, TX 76798, USA
* Correspondence: khalotaibi@ksu.edu.sa

Abstract: Date palm trees generate large amounts of various types of waste, including leaf sheath fibres, which can be used as a low-cost precursor for the production of biochar, including activated carbon (AC), which can be employed for the adsorption of contaminants. In the current study, activated carbon was produced from leaf sheath fibres of date palms (LSDPFAC) by the use of chemical activation with K_2CO_3 combined with microwave irradiation, and it was characterised and evaluated for its adsorptive capacity of lead ions (Pb^{2+}). The Brunauer–Emmett–Teller (BET) surface area, Langmuir surface area, total pore volume and average pore diameter of the LSDPFAC were 560.20 m^2/g, 744.31 m^2/g, 0.29 cm^3/g and 2.47 nm, respectively. A greater adsorption of Pb^{2+} was observed when its concentration was higher in the solution, and the greatest adsorption capacity of 5.67 mg Pb/g was observed at the highest pH. The results of isotherm and kinetic studies demonstrated that the adsorption of Pb^{2+} onto the LSDPFAC was best described by the Freundlich isotherm and pseudo-second-order (PSO) models. The Langmuir ΔG° and E_a were 6.39 kJ/mol, 0.12 kJ/mol K, −31.28 kJ/mol and 15.90 kJ/mol, respectively, which demonstrated that the adsorption of Pb^{2+} by the LSDPFAC was endothermic, spontaneous and governed by physisorption.

Keywords: activated carbon; metal ions; *Phoenix dactylifera* L.; isotherm; kinetic; microwave irradiation; biochar

check for updates

Citation: Aloud, S.S.; Hameed, B.H.; Yusop, M.F.M.; Alharbi, H.A.; Giesy, J.P.; Alotaibi, K.D. Adsorption of Pb^{2+} by Activated Carbon Produced by Microwave-Assisted K_2CO_3 Activation of Date Palm Leaf Sheath Fibres. *Water* **2023**, *15*, 3905. https://doi.org/10.3390/w15223905

Academic Editors: Alessandro Erto and Yulin Tang

Received: 2 September 2023
Revised: 21 October 2023
Accepted: 24 October 2023
Published: 8 November 2023

1. Introduction

Due to the presence of pollutants in water supplies around the globe, more than 700 million people do not have access to safe drinkable water [1]. Some of the most common water contaminants are metals, including lead (Pb), zinc (Zn), nickel (Ni), cadmium (Cd), chromium (Cr), copper (Cu), arsenic (As) and mercury (Hg). Although most countries have promulgated the maximum permissible concentrations of metals in surface waters, under realistic situations, these rules are difficult to enforce [2,3]. When present at concentrations that exceed permissible concentrations, these metals can cause adverse effects and impart serious health problems to humans, such as damaging kidneys, nerve tissues and the liver. Furthermore, they can cause cancer in vital organs, including the bladder, skin and lungs [4–6]. In addition, metals are able to cause various illnesses in the bones, muscles, fat and joints of people [7]. One of the most hazardous metals is lead (Pb^{2+}), which is released to the lithosphere during processes including metallurgy mining, lead–acid battery manufacturing, vehicle exhaust and tin–lead soldering in domestic pipes [8]. Lead has been directly connected to severe diseases, including pathology of the liver, malfunction of the kidney, rupture of the central nervous system and infertility [9–11]. Moreover, Pb^{2+} is associated with diseases like encephalopathy and anaemia [12].

There are a range of methods employed to remove Pb^{2+} from water, including ion exchange [13], electro-chemical [14], electro-dialysis [15], membrane filtration [16] and biological processes [17]. Furthermore, adsorption using activated carbon (AC) is another method that has been described as one of the best methods for the removal of Pb^{2+}. First, since equilibrium can be obtained in as little as 45 min, this method is fast [18]. Second, the adsorption is versatile and can adsorb a range of contaminants, including metals [19,20], dyes [21–23], caffeine [24], pesticides [25], carbon dioxide [26] and others. Third, since biochar can be derived from low-cost biomass wastes, such as jackfruit peels, [27], corn fibres [28], orange peels [29], teak wood [30], date palm bark wastes [31], cocoa shells [32], acacia wood [33], mango seeds [34] and others that can be converted into activated carbon, the process of adsorption is relatively easy and economically feasible. Utilising agricultural waste to produce activated carbon is a valuable solution to the substantial and costly issue of disposing of agricultural by-products, ultimately converting them into high-value sorbents with enhanced utility [35]. Furthermore, activated carbon used for adsorption can target specific types of contaminants [36].

Producing activated carbon involves two main steps: carbonisation followed by activation. During carbonisation, a precursor material is turned into char through pyrolysis under an inert gas at temperatures between 300 and 500 °C. Then, in the activation step, char is transformed into activated carbon through physical activation, chemical activation or a combination of both. Physical and physicochemical activation typically use higher temperatures, ranging from 700 to 900 °C, while chemical activation uses lower temperatures, between 400 and 600 °C. The heat needed for activation can come from a regular furnace or from microwaves. Using microwaves can speed the activation significantly, making it as much as 20 times faster without sacrificing the quality of the activated carbon produced [37]. During microwave heating, the samples absorb microwave energy, causing certain compounds in the samples to vibrate very quickly, generating heat that activates the samples [38].

In this study, waste from date palms (date palm leaf sheath fibres) was used to produce AC (LSDPFAC), and its efficiency for adsorbing Pb^{2+} from an aqueous solution was evaluated. The date palm (*Phoenix dactylifera* L.) is a tree that belongs to the family of *Arecaceae* and is largely cultivated in Middle Eastern and North African countries [39,40]. In addition to the production of edible fruits, the date palm tree produces large amounts of agricultural waste. For instance, one date palm tree can produce up to 40 kg of waste per year, including dried leaves, sheaths, spathes and petioles [41]. AC derived from date palm leaf sheath fibres has been shown to effectively remove dye from aqueous solutions [42], and its efficiency for adsorbing heavy metals deserves further investigation. The utilisation of date palm leaf sheath fibres for the production of AC can reduce the amount of generated date palm waste in addition to saving the environment by adsorbing Pb^{2+} pollutants from aqueous solutions. Therefore, the objective of the current study was to produce AC from date palm leaf sheath fibres as a low-cost precursor via activation with K_2CO_3 under microwave heating for Pb^{2+} adsorption from aqueous solutions. The adsorption of Pb^{2+} onto the LSDPFAC was studied in terms of an equilibrium study (effect of different initial concentrations, effect of different solution temperatures and effect of the solution pH) in addition to an evaluation of the isotherm, kinetic and thermodynamic properties. To the best of our knowledge, this study is the first to activate date palm leaf sheath fibres using K_2CO_3 coupled with the microwave heating technique. Also, another novelty of this study was employing the Dubinin–Radushkevich model to understand the mechanism of the adsorption process. This fundamental research will offer valuable insights for developing an adsorbent aimed at treating effluents containing Pb^{2+} [43] in the future.

2. Materials and Methods

2.1. Materials

The precursor leaf sheath date palm fibres were acquired from a private farm near Riyadh city, Saudi Arabia. Potassium carbonate, K_2CO_3, which was used as chemical activating agent was purchased from Sigma Aldrich Inc. (St. Louis, MO, USA), while 0.10 M hydrochloric acid, HCl, was bought from R&M Chemicals, Petaling Jaya, Selangor, Malaysia. Synthetic wastewater was prepared by using lead nitrate, $Pb(NO_3)_2$ (assay > 99.0), which was purchased from Sigma Aldrich. Nitrogen gas, N_2 (purity of 99.9%), was supplied by Linde Malaysia Sdn Bhd, Petaling Jaya, Selangor, Malaysia.

2.2. Preparation of Activated Carbon (LSDPFAC) from Leaf Sheath Fibres from Date Palm

Once obtained, the precursor fibres of leaf sheath from date palm were first dried in open air, chopped into small pieces and finely ground to reach a particle size of 1–2 mm. These materials were transferred to the lab, cleaned with water and placed in an oven at 110 °C for 48 h to dry. The dried precursor was saturated with K_2CO_3 at a ratio of 1:3. The impregnated sample was once again stored in an oven at 50 °C for 24 h. At this point the material was heated using a modified microwave oven (EMW2001W, Sweden) at a radiation power of 616 Watts for 10 min. An anoxic atmosphere was created by passing N_2 gas through the container of the sample at 80 cm^3/min. After heating was complete, the sample, which at that point had been transformed to LSDPFAC, was cooled. The LSDPFAC was soaked in 0.10 M HCl for 30 min and then rinsed with warm water until the washing solution pH became 6–7. The wet LSDPFAC was heated in an oven at 110 °C for 24 h. Once dried, the LSDPFAC was kept inside an air-tight container until use for the adsorption studies and characterisation tests.

2.3. Characterisation Methods

The LSDPFAC was characterised in terms of various parameters. The surface area was estimated by the use of the Brunauer–Emmett–Teller (BET) method and the Langmuir function, and the pore characteristics, including the total pore volume and average pore size, of the LSDPFAC were determined by a volumetric adsorption analyser (USA). The surface morphology was examined by the use of a scanning electron microscope (SEM) (model: LEO SUPRA 55VP, Zeiss, Oberkochen, Germany). Analysis of the elemental composition was achieved by the use of a simultaneous thermal analyser (STA) (Perkin Elmer STA 6000, Waltham, MA, USA), and proximate analysis was carried out by a thermogravimetric analyser (TGA). Surface chemistry analyses were conducted by using a Fourier transform infrared (FTIR) spectroscope (model: IR Prestige 21, Shimadzu, Japan). The distribution of the zeta potential was acquired by employing a zeta potential analyser (Model: Zetasizer Nano Series DKSH, Petaling Jaya, Selangor, Malaysia).

2.4. Equilibrium Study

Six concentrations of Pb^{2+}, ranging from 1 to 10 mg/L, were used to investigate the adsorption capacity of the LSDPFAC vs the concentration at equilibrium. Solutions with the target concentrations were prepared in conical flasks. A relatively small concentration of Pb^{2+} was chosen since the adsorption of adsorbate at these ranges is challenging. At lesser concentrations of adsorbate, the driving force that promotes adsorption is weaker. The volume of each of these solutions was 200 mL. All conical flasks were placed in a water bath shaker. Next, accurately weighed 0.2 g amounts of LSDPFAC were added to each conical flask, and the mouths were sealed with film to prevent evaporation. The temperature of the water bath shaker was 30 °C, and the shaking speed was 60 rpm. Every 30 min, samples of the Pb^{2+} solutions were withdrawn using a syringe, and their concentrations were determined by the use of UV-Vis spectrophotometry (model: Agilent Cary 60, Santa

Clara, CA, USA). This process was continued until steady state was achieved. The second parameter investigated was the temperature, for which the adsorption process was tested at 30, 40 and 50 °C at a constant pH. The pH of the Pb^{2+} solution was adjusted to 3, 4, 5 or 6 by the use of HCl or NaOH, with the temperature being fixed at 30 °C. Other experimental conditions were fixed as follows: (i) solution volume of 200 mL, (ii) adsorbent weight of 0.2 g and (iii) shaking speed of 60 rpm. The capacity of the LSDPFAC to absorb Pb^{2+} and the percentage removal of Pb^{2+} by the LSDPFAC were determined as follows (Equations (1) and (2)):

$$q_e = \frac{(C_o - C_e)V}{M} \tag{1}$$

$$Removal\ (\%) = \frac{(C_o - C_e)}{C_o} \times 100\% \tag{2}$$

where q_e refers to the amount of Pb^{2+} ions adsorbed by the LSDPFAC at the equilibrium state (mg/g), C_o and C_e refer to the Pb^{2+} concentrations at the initial state (mg/L) and equilibrium state (mg/L), respectively, V refers to the volume of the Pb^{2+} solution and M refers to the weight of LSDPFAC (g).

2.5. Isotherm Study

Information about the connection between the adsorbate concentration in the bulk phase and the adsorbate concentration in the solid phase can be determined by studying isotherm models. Hence, the two most popular isotherm models, i.e., the Langmuir [44] (Equation (3)), Freundlich [45] (Equation (4)) and Dubinin–Radushkevich [46] models, were used to describe the isotherms as follows (Equations (5)–(7)):

$$q_e = \frac{Q_m K_L C_e}{1 + K_L C_e} \tag{3}$$

$$q_e = K_F C_e^{1/n_F} \tag{4}$$

$$q_e = Q_{DR} \exp\left(-B_{DR}\varepsilon^2\right) \tag{5}$$

$$\varepsilon = RT \ln\left(1 + \frac{1}{C_e}\right) \tag{6}$$

$$E_{DR} = \left(\frac{1}{\sqrt{2B_{DR}}}\right) \tag{7}$$

where Q_m refers to the Langmuir maximum monolayer adsorption capacity (mg/g), K_L refers to a parameter that is related to the energy of adsorption (L/mg), K_F refers to the constant of the adsorption process (mg/g) $(L/mg)^{1/n}$, n_F refers to the heterogeneity parameter, R refers to the universal gas constant with a fixed value of 8.314 J/mol, Q_{DR} is the maximum adsorption capacity (mg/g), B_{DR} is a constant related to the adsorption energy (mol^2/kJ^2) and EDR is the adsorption energy (kJ/mol). K and T are the temperature of the adsorbate solution (K). To fit the non-linear equations of the isotherm models, Microsoft Excel Solver v. 2016 was used. The model that best fit the adsorption data was chosen based on the correlation coefficient, R^2, as well as the root mean squared error (RMSE). The value of RMSE was calculated as follows (Equation (8)) [47]:

$$RMSE = \sqrt{\frac{1}{n-1}\sum_{n=1}^{n}\left(q_{e,exp,n} - q_{e,cal,n}\right)^2} \tag{8}$$

2.6. Kinetic Study

The same procedure as that used for the equilibrium study was performed in the kinetic study, except that in the kinetic study, the concentrations of Pb^{2+} were determined at a pre-determined time between 0 to 180 min. The two most popular kinetic models, i.e., the pseudo-first-order (PFO) [48] (Equation (9)) and pseudo-second-order (PSO) [49] (Equation (10)) models, were both applied as follows:

$$q_t = q_e[1 - exp(-k_1 t)] \tag{9}$$

$$q_t = \frac{k_2 q_e^2 t}{1 + k_2 q_e t} \tag{10}$$

where k_1 and k_2 refer to the rate constant obtained from the PFO model (1/min) and the rate constant obtained from PSO model (g/mg min), respectively. The kinetic model that best described the adsorption data was judged based on the R^2 and RMSE values.

2.7. Thermodynamic Study

Since the solution temperature influences the adsorbate–adsorbent interactivity during the adsorption process, these effects can be fully understood by conducting a thermodynamic study. There are 4 important thermodynamic parameters: the enthalpy change, ΔH°, the entropy change, ΔS°, the Gibbs free energy, ΔG°, and the Arrhenius activation energy, E_a. To determine the values of ΔH° (kJ/mol) and ΔS° (kJ/mol K), the relationships among these parameters can be described by the van't Hoff equation (Equation (11)):

$$ln\ K_c = \frac{\Delta S^\circ}{R} - \frac{\Delta H^\circ}{RT} \tag{11}$$

where R denotes the universal gas constant with a fixed value of 8.314 J/mol K, T refers to the solution temperature (K) and K_c is a dimensionless parameter that is recognised as the equilibrium constant. The value of K_c can be calculated from the following equation [50] (Equation (12)):

$$K_c = \frac{1000\frac{mg}{g} \times K_L \times molecular\ weight\ of\ adsorbate \times [adsorbate]^\circ}{\gamma} \tag{12}$$

where [adsorbate] is the adsorbate standard concentration, where the value of this parameter can be presumed to be 1 mol/L at a standard condition, γ is a dimensionless parameter that refers to the activity coefficient for the studied adsorbate and KL is the adsorption constant obtained from the Langmuir isotherm model (L/mg). On the other hand, the following formulas shown below were utilised to find the other two thermodynamic parameters, namely ΔG° (kJ/mol) (Equation (13)) and E_a (kJ/mol) (Equation (14)), respectively:

$$\Delta G^\circ = \Delta H^\circ - T\Delta S^\circ \tag{13}$$

$$ln\ k_2 = ln\ A - \frac{E_a}{RT} \tag{14}$$

where k_2 refers to the rate constant obtained from the PSO kinetic model (g/mg min), and A represents the Arrhenius factor. All the adsorption experiments in this study were replicated three times, and the average values were used.

3. Results and Discussion

3.1. Characteristics of Samples

The LSDPFAC had a BET surface area of 560.20 m^2/g and a Langmuir surface area of 744.31 m^2/g. This value of the BET surface area was similar to that of AC derived from acacia wood (AWAC), which had a BET of 1045.56 m^2/g [33]. This was because unlike AWAC, the LSDPFAC in this study was synthesised with a chemical treatment without undergoing an initial carbonisation. Carbonisation is known to aid in the formation of a network of pores during the initial stages of the formation of AC. Nonetheless, the decision to omit the carbonisation stage in producing the LSDPFAC in this study was justified by the fact that the process of producing the LSDPFAC simpler and required one less step, and due to the usage of N_2 gas instead of CO_2 gas during the microwave heating treatment, it was deemed to be more environmentally compatible. The mean BET surface area of the LSDPFAC was produced by the relatively moderate radiation power (616 Watts) employed in this study. A previous study (Hijab et al. [51]) succeeded in producing AC with a relatively larger surface area of 1123 m^2/g from date stones by using radiation power at 850 W. The creation of the surface area in the LSDPFAC was initially contributed to by the chemical agent (K_2CO_3) that penetrated the external layer of the precursor to create a network of pores. During the microwave activation, the K_2CO_3 enhanced the degradation of polar components, such as cellulose and lignin, in the date palm material [52]. The total pore volume of the LSDPFAC was 0.29 cm^3/g, while the mean diameter of the pores was 2.47 nm. Since this value is between 2 to 50 nm, the pores in the LSDPFAC were verified to be of a mesopore type. Despite using a moderate radiation power of 616 Watts and the omission of a carbonisation step, the LSDPFAC still contained mesopores, which validated the use of K_2CO_3.

The precursor used in this study was confirmed to be appropriate because it had a carbon content of 33.45% and a relatively large proportion of fixed carbon of 19.92% (Table 1). In comparison, the fixed carbon amount in other biomass materials has been shown to be 18.82% for durian shell [53], 17.10% for almond shell [54], 14.06% for karanja fruit hull [55] and 18.12% for coffee husk [54]. Chemical activation by K_2CO_3 coupled with microwave heating effectively removed moisture and volatile components from the date palm materials. In the LSDPFAC, the proportion of elemental carbon increased to 55.67%, and that of fixed carbon increased significantly to 76.52%. Conversely, the proximate analysis showed that the amount of volatile matter decreased from 66.27 to 5.99%. During the microwave heating, moisture and other polar components inside the sample absorbed the microwave energy and vibrated more rapidly, which caused heat to be dissipated. Heat then caused the volatile matter to evaporate and leave the sample. The amount of moisture increased from 11.92 to 14.26% after the chemical treatment and microwave heating. This increment occurred in terms of percentage only and did not reflect an actual increase in the absolute amount of moisture. The moisture came from the addition of deionised water to mix the sample and K_2CO_3 during the chemical activation stage.

Table 1. Elemental and proximate analysis of samples.

Samples	Elemental Analysis					Proximate Analysis			
	C	**H**	**N**	**S**	**Others**	**Moisture**	**Volatile Matter**	**Fixed Carbon**	**Ash**
Precursor	33.45	3.85	0.97	0.37	61.36	11.92	66.27	19.92	1.90
LSDPFAC	55.67	5.44	0.74	0.37	37.78	14.26	5.99	76.52	3.23

At a magnification of 5000× in the SEM images of the precursor materials and the LSDPFAC, the surface of the precursor was seen to be rough and dense and contained no pores The magnification level of the SEM images of the precursor and LSDPFAC was 5000× (Figure 1). The pores in the LSDPFAC were initially occupied by the typical components of lignocellulosic materials, such as cellulose, hemicellulose and lignin [56], which were subsequently removed, which resulted in the formation of the network of pores in the LSDPFAC.

The surface of the AC carried a net charge, which was a function of the precursor used in this study and the activation steps applied during the synthesis of the AC. Since adsorption is a surface phenomenon, CV can influence adsorption. This net charge can be verified from the distribution of the zeta potential [57] (Figure 2a). The zeta potential of the LSDPFAC was −25.5 mV, which indicated that the LSDPFAC carried a net negative charge on its surface. AC generally carries a net zeta potential, which is more efficient for adsorbing a positive charge [33].

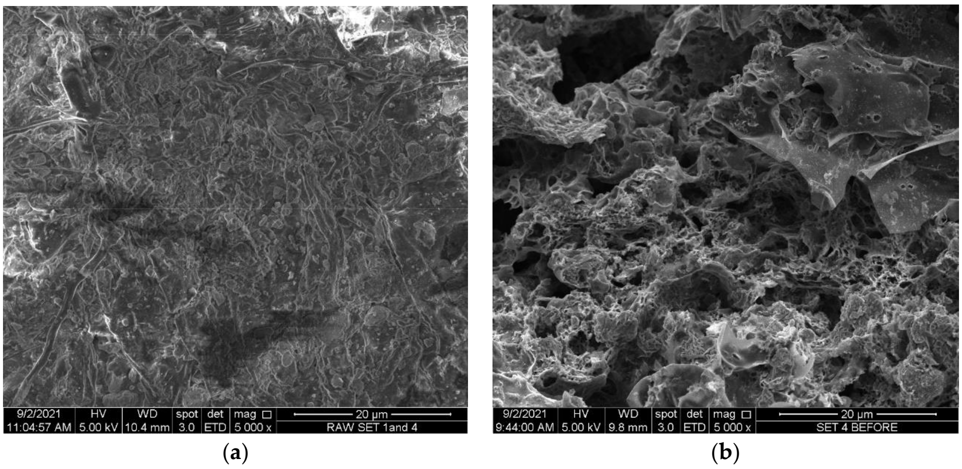

Figure 1. SEM images of (**a**) precursor material and (**b**) LSDLFAC (5000× magnification).

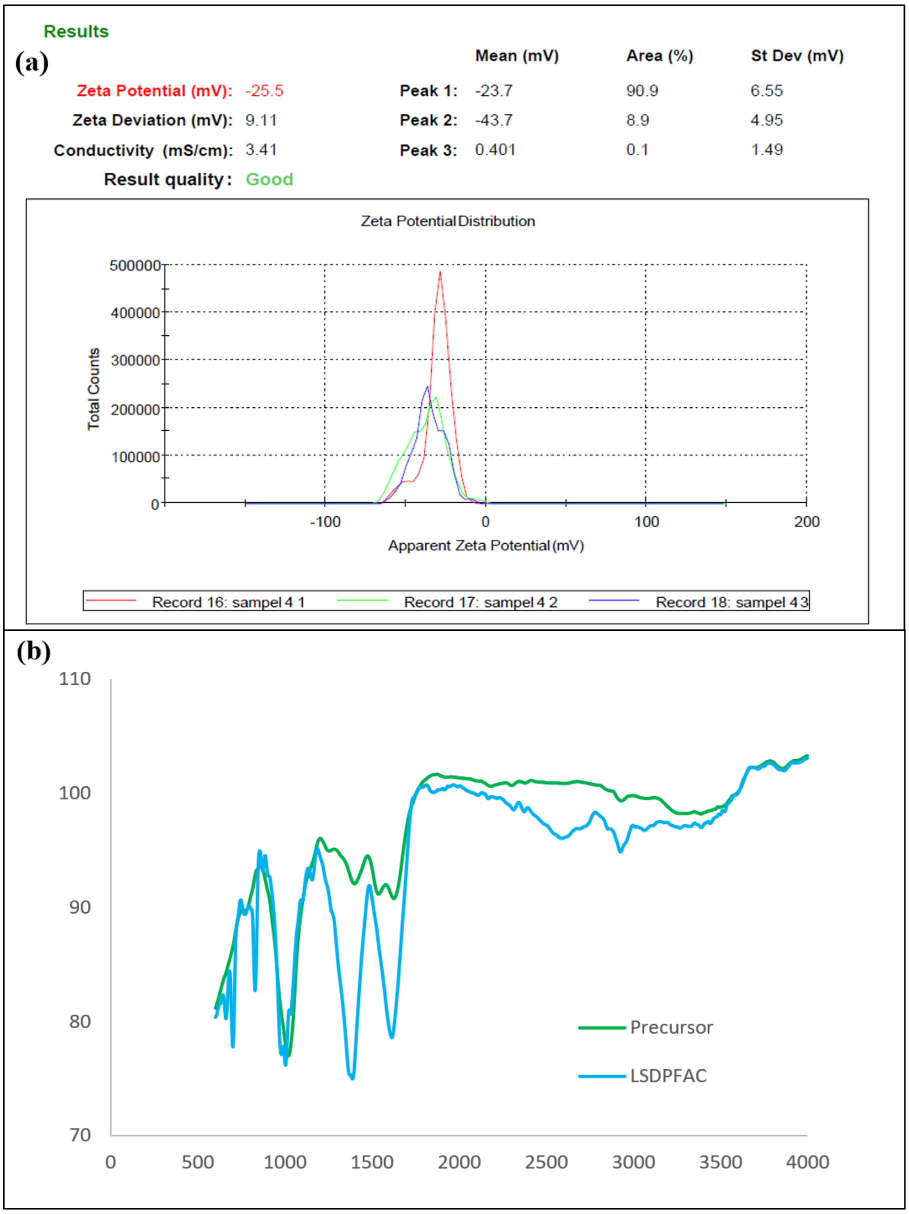

Figure 2. Zeta potential of LSDPFAC (**a**) and FTIR spectra of precursor materials and LSDPFAC (**b**).

The surface of the precursor material was filled with functional groups of methylene $(CH_2)_n$, which was determined by the presence of an FTIR peak of 748 cm^{-1}, which was indicative of aromatic ring, C=C-C, stretching at a peak of 1583 cm^{-1}, methyl, C-H, asymmetric stretching at 2970 cm^{-1} and nonbonded hydroxy group, OH, stretching at 3645 cm^{-1} (Figure 2b and Table 2). These functional groups did not appear on the surface of the LSDPFAC and were removed during the activation steps. Some functional groups survived the activation steps and thus appeared in both the surfaces of the precursor and the LSDPFAC. These functional groups were peroxide, C-O-O-, stretching, which appeared at 860 cm^{-1} in the precursor and at 856 and 881 cm^{-1} in the LSDPFAC, and phenol, which appeared at 1199 and 1198 cm^{-1} in the precursor and LSDPFAC, respectively. Some new peaks, such as tertiary alcohol, C-O, stretching at 1148 cm^{-1} and carbonate ions at 1477 cm^{-1}, were observed on the LSDPFAC. The carbonate ions came from the K_2CO_3 utilised during the chemical activation step.

Table 2. Diagnostic peaks in FTIR spectra of precursor materials and PFAC.

Precursor		LSDPFAC	
Peak (cm^{-1})	**Functional Groups**	**Peak (cm^{-1})**	**Functional Groups**
748	Methylene –(CH2)n	648	Alkyne, C-H, bending
860	Peroxides, C-O-O-, stretching	677	Alkyne, C-H, bending
1199	Phenol, C-O, stretching	856	Peroxides, C-O-O-, stretching
1583	C=C-C Aromatic ring stretching	881	Peroxides, C-O-O-, stretching
2970	Methyl, C-H, asymmetric stretching	1148	Tertiary alcohol, C-O, stretching
3645	Nonbonded hydroxy group, OH, stretching	1198	Phenol, C-O, stretching
		1477	Carbonate ions

3.2. Adsorption Equilibrium

The effect of the contact duration at various concentrations on the adsorption of Pb^{2+} is shown in Figure 3. The Pb^{2+} adsorption uptake values increased as its concentration increased in the solution. At higher Pb^{2+} concentrations, more Pb^{2+} ions were available for absorption by the LSDPFAC, indicating a greater adsorption of Pb^{2+} with greater concentrations of Pb^{2+}.

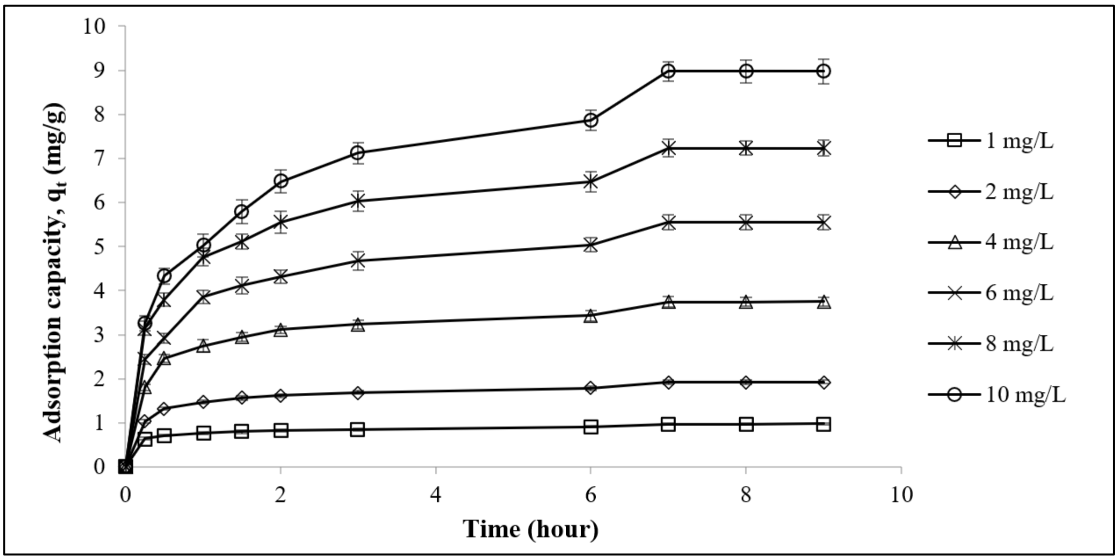

Figure 3. Adsorption of Pb^{2+} by LSDPFAC versus time at 30 °C for different concentrations.

The greatest adsorption of 5.76 mg Pb^{2+}/g by the LSDPFAC was obtained at pH 6. As the pH decreased to 5, the Pb^{2+} uptake reduced to 4.85 mg/g. At pH 5, the presence of more H^+ ions in the solution induced the surface of the LSDPFAC to be positively charged. The positively charged LSDPFAC's surface repelled the Pb^{2+} ions. As the solution pH decreased to 4 and 3, the repulsion between the LSDPFAC's surface and the Pb^{2+} ions became more intense, hence the Pb^{2+} uptake values decreased further to 4.63 and 4.51 mg/g, respectively. The adsorption of Pb^{2+} by the LSDPFAC at pH 7 and above could not be determined because at these pH values, the solution was dominated by $Pb(OH)^+$ and $Pb_3(OH)_4{}^{2+}$.

3.3. Adsorption Isotherm

The adsorption of Pb^{2+} by the LSDPFAC could best be described by the Freundlich model (R^2 = 0.9972; RMSE = 0.11 (Table 3; Figure 4b). Thus, the Pb^{2+} ions formed a multilayer coverage on the surface of the LSDPFAC. The maximum monolayer adsorption capacity, Q_m, was 14.10 mg/g, which was comparable to other findings, such as the adsorption of Pb^{2+} by leaf-extract-derived ZnO nanoparticles, which was 16.26 mg/g [58], and that of rice-husk-derived biochar, which was 22 mg/g [59]. Since the heterogeneity factor, n, for the adsorption of PB^{2+} by ^{the} LSDPFAC, which was 1.69 was between 1.0 and 10, the adsorption of PB^{2+} was favourable [33]. The use of the Dubinin–Radushkevich model was important in verifying the mechanism involved in the adsorption process [46]. This model is commonly employed for distinguishing between physical and chemical adsorption. This is achieved by utilising the constant B_{DR} to gauge the sorption energy, E_{DR}. Physical adsorption is typically inferred when the E_{DR} is below 8 kJ/mol. In cases where the E_{DR} falls between 8 and 16 kJ/mol, it is generally presumed that chemisorption is occurring [60]. In this study, the E_{DR} value obtained was 3.17 kJ/mol, thus confirming that the mechanism was physical adsorption. The Langmuir model can be utilised to find the separation factor, R_L (dimensionless) (Equation (15)), as follows:

$$R_L = \frac{1}{1 + K_L C_o} \tag{15}$$

The R_L parameter is important in verifying the favourability of the adsorption process. If the R_L value is > 1, the adsorption process is unfavourable; if R_L = 1, the adsorption process is linear; if R_L is between 0 and 1, the adsorption process is favourable; and if R_L = 0, the adsorption process is irreversible [61]. The R_L values obtained for this study were between 0.064 and 0.41, signifying that the adsorption process at all the initial concentration studied was favourable.

Table 3. Isotherm parameters for Pb^{2+}–LSDLFAC adsorption system at 30 °C.

Isotherm	Parameters	30 °C
Langmuir	Q_m	14.10
	K_L	1.21
	R_L	0.064–0.41
	R^2	0.9976
	RMSE	0.35
Freundlich	K	7.65
	n	1.69
	R^2	0.9972
	RMSE	0.11
Dubinin–Radushkevich	Q_{DR}	9.46
	B_{DR}	0.05
	E_{DR}	3.17
	R^2	0.9939
	RMSE	0.48

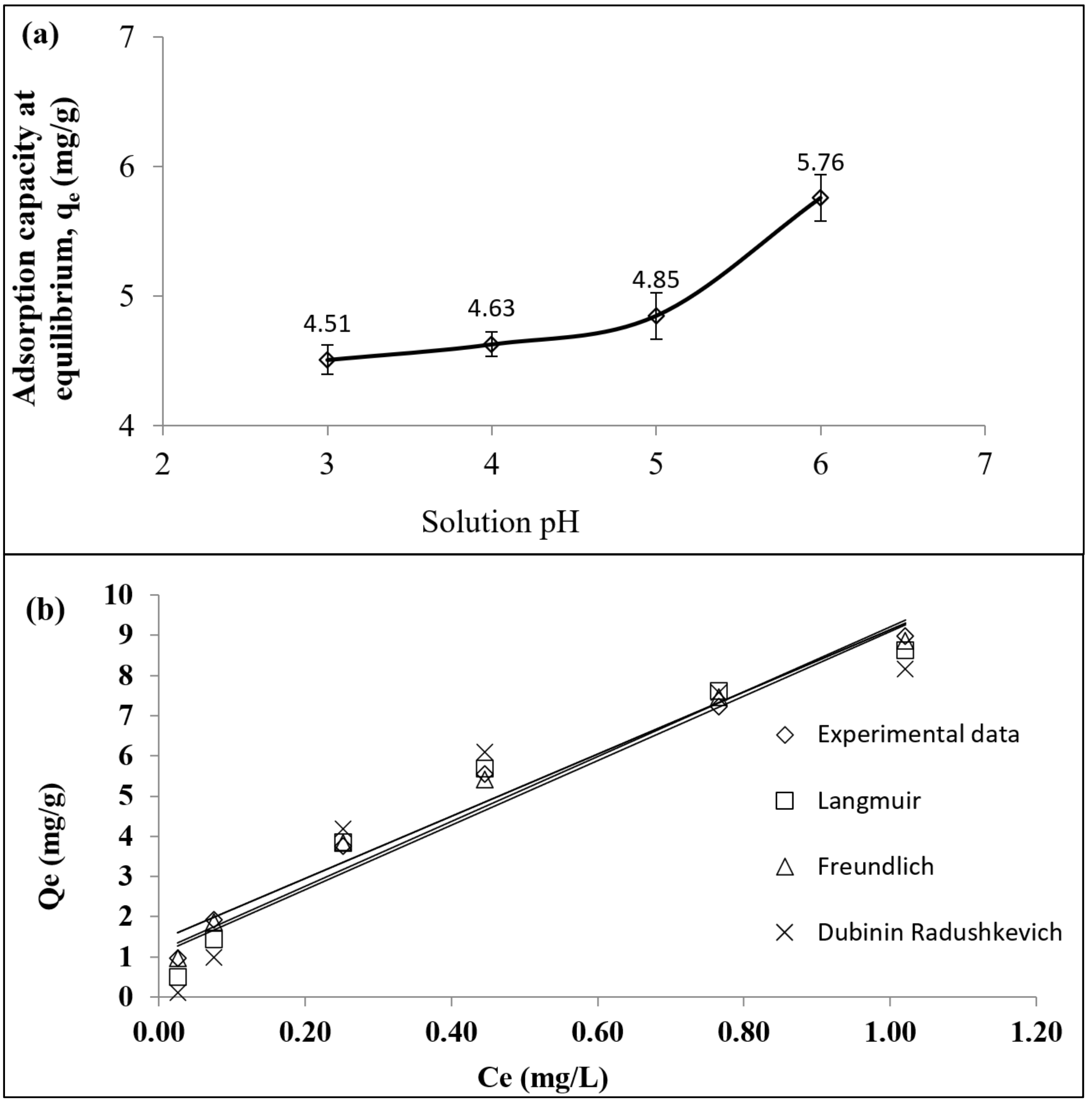

Figure 4. Plots of Pb^{2+} adsorption uptakes by LSDPFAC versus solution pH at 30 °C (10 mg/L concentration, 0.2 g adsorbent dosage and 200 mL of solution) (**a**) and plots of isotherm models for Pb^{2+}–LSDLFAC adsorption system at 30 °C (**b**).

3.4. Adsorption Kinetics

The kinetics of the adsorption of Pb^{2+} onto the LSDPFAC was best described by the PSO model (Figure 5a,b). The RMSE value of the PSO model of 0.14 was less than that of the PFO model, which was 0.30 (Table S1). The adsorption of Pb^{2+} by AC produced from cigarette waste [18] and by AC derived from mangosteen peel [20] were also best described by the PSO model. A consistent decreasing trend was observed in the k_2 values (from 0.1735 to 0.0043 g mg^{-1} min^{-1}) as the initial Pb^{2+} concentration increased from 1 to 10 mg/L. At greater concentrations of Pb^{2+}, the presence of many Pb^{2+} ions in the solution created a lot of competition for the adsorption process to occur. In order to understand the mechanism of the adsorption process better, the Boyd plot was constructed and is given in Figure 6. All the lines in the Boyd plots were noted to not pass through the origin point. Therefore, it can be concluded that the rate-determining step in the adsorption process was the film diffusion mechanism [30]. For comparison purposes between this study and other studies, Table 4 provides a summary of the data of Pb^{2+} adsorption systems with different types of adsorbents.

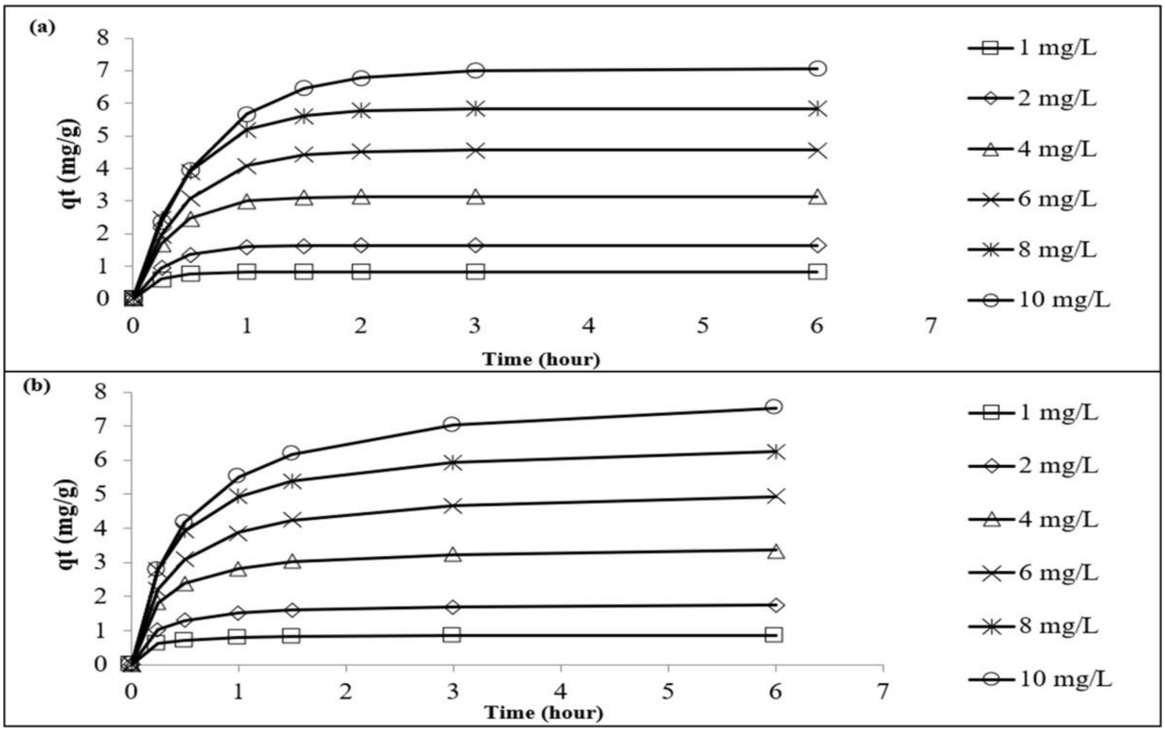

Figure 5. Plots of pseudo-first-order kinetic model for Pb^{2+}–LSDLFAC adsorption system at 30 °C (**a**) and plots of pseudo-second-order kinetic model for Pb^{2+}–LSDLFAC adsorption system at 30 °C (**b**).

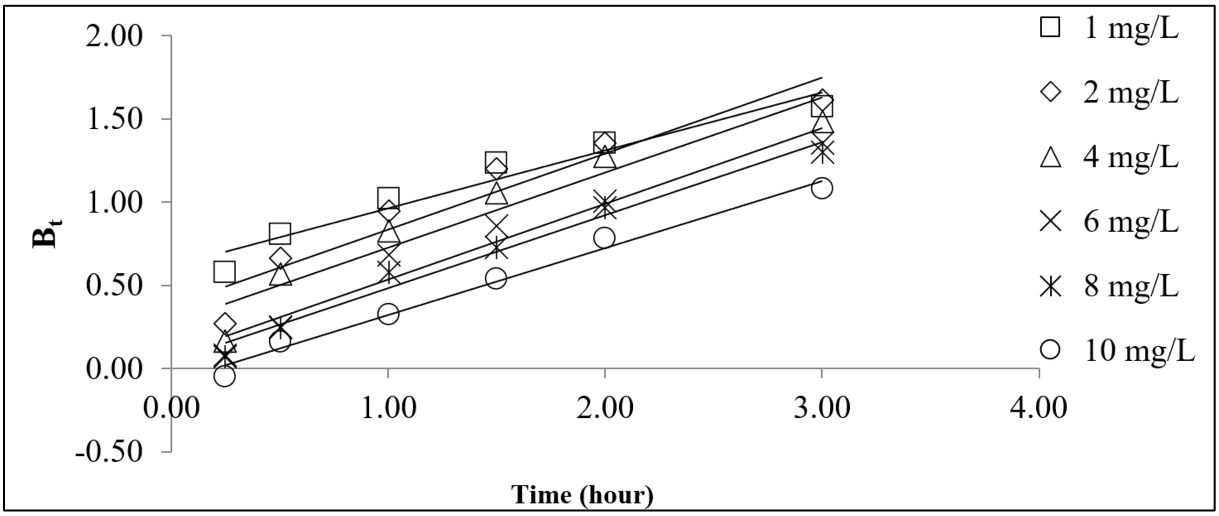

Figure 6. Boyd plots for Pb^{2+}–LSDLFAC adsorption system at 30 °C.

3.5. Adsorption Thermodynamics

The thermodynamic nature of the adsorption process can be evaluated by conducting the adsorption process at various temperatures (Figure 7) (Table S2). For instance, when the solution temperature increased from 30 to 50 °C, the adsorption of Pb^{2+} increased from 8.76 to 8.98 mg/g, which indicated an endothermic adsorption of Pb^{2+} by the LS-DPFAC (Figure 7), which was consistent with the positive value of ΔH° of 6.39 kJ/mol. Similarly, the adsorptions of Cu^{2+}, Pb^{2+}, Cd^{2+} and Zn^{2+} ions by an AC-supported silver–silica nanocomposite were all endothermic [69]. The positive ΔS° value of 0.12 kJ/mol K indicated an increment of randomness at the liquid–solid interface. The value of E_a, which was 15.90 kJ/mol, was less than 40 kJ/mol, suggesting that the adsorption of Pb^{2+} by the LSDPFAC was physically governed [70]. The negative ΔG° values of −31.28,

−32.53 and −33.77 kJ/mol at temperatures of 303.15, 313.15 and 323.15 K, respectively, indicate that the adsorption of Pb^{2+} onto the LSDPFAC occurred in a spontaneous manner at all temperatures.

Table 4. Comparison of adsorption processes for different types of heavy metals by different types of adsorbents.

Adsorbent	Isotherm	Kinetic	Langmuir Monolayer Adsorption Capacity, Q_m (mg/g)	Rate Constant	Mechanism	Experimental Conditions	References
Leaf sheath fibre of date-palm-based activated carbon	Freundlich	PSO	14.10	0.1735 to 0.0043 g mg^{-1} min^{-1}	Physisorption	Concentration: 1–10 mg/L pH: 3–9	This study
Composite track-etched membranes	Freundlich	PSO	0.08–0.21	0.09 × 10^{-4}–0.55 × 10^{-4} g μg^{-1} min^{-1}	Ion exchange and chemisorption	Concentration: 50 mg/L pH: 3–8	[62]
Biomass-derived activated carbon supported by nano zero-valent iron particles	Langmuir–Freundlich	PSO	23.30–140.80	0.006 g mg^{-1} min^{-1}	Surface and redox reaction	Concentration: 10–1000 mg/L pH: 2–10	[63]
Mango seed biosorbent	Redlich–Peterson	PFO	283.20	0.461 min^{-1}	Electrostatic attraction, micro-precipitation, complexation and ion exchange	Concentration: 500 mg/L pH: 2–7.5	[64]
Molybdenum sulphide (MoS_2)/thiol-functionalised multiwalled carbon nanotube	Freundlich	PSO	90.00	0.014 g mg^{-1} min^{-1}	Ion exchange and electrostatic interactions	Concentration: 100 mg/L pH: 2–6	[65]
Magnetic nickel-ferrite nanoparticles	-	PSO	-	0.0148 g mg^{-1} min^{-1}	-	Concentration: 5 mg/L pH: 2–6	[66]
Zinc oxide (ZnO) and copper (II) oxide (CuO) nanoparticles	Freundlich	PSO	-	1.97 × 10^{-4}–2.09 × 10^{-4} g mg^{-1} min^{-1}	Chemical interactions	Concentration: 100 mg/L pH: 3–9	[67]
A. compressa K.-based activated carbon	Langmuir	PSO	170.00	0.488–3.175 to 0.022–0.032 g mg^{-1} min^{-1}	Chemisorption	Concentration: 25–250 mg/L pH: 2–6	[68]

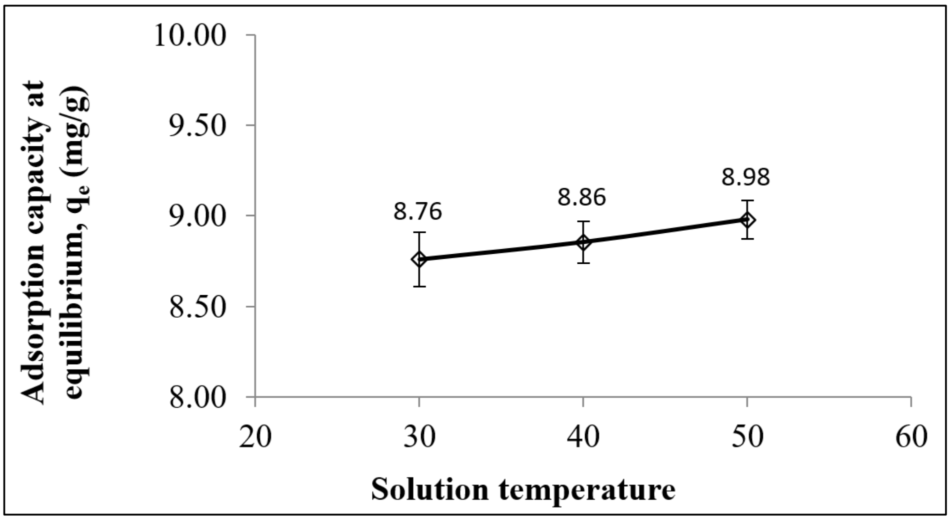

Figure 7. Adsorption capacity of Pb^{2+} onto LSDPFAC versus different solution temperatures.

4. Conclusions

Date palm leaf sheath fibre was effectively converted into activated carbon (LSDPFAC) and utilised for the removal of Pb^{2+} ions from aqueous solutions. The LSDPFAC exhibited BET and Langmuir surface areas of 560.20 m^2/g and 744.31 m^2/g, respectively. The LSDPFAC posed mesopore-type pores due to it having an average pore diameter of 2.47 nm with a total pore volume of 0.29 cm^3/g. The FTIR spectrum indicated that the surface of the LSDPFAC was occupied by alkyne, C-H, bending, peroxides, C-O-O, stretching, tertiary alcohol, C-O, stretching, and phenol, C-O, stretching. A higher Pb^{2+} adsorption occurred at higher Pb^{2+} concentrations and vice versa. The highest adsorption of Pb^{2+} took place at pH 6 (5.76 mg/g) and at temperature 50 °C (8.98 mg/g). The adsorption of Pb^{2+} onto the LSDPFAC obeyed the Freundlich isotherm model and PSO kinetic model. The adsorption energy, E_{DR}, obtained from the Dubinin–Radushkevich model confirmed that the adsorption process was controlled by the physisorption mechanism. The Boyd plot confirmed that the rate-limiting step was caused by the film diffusion mechanism. Date palm leaf sheath fibre shows promising potential as an alternative low-cost precursor.

Supplementary Materials: The following are available online at https://www.mdpi.com/article/10.3390/w15223905/s1, Table S1: Kinetic parameters for Pb^{2+}–LSDPFAC adsorption system, Table S2: Thermodynamic parameters.

Author Contributions: Conceptualisation, S.S.A. and B.H.H.; methodology, S.S.A., B.H.H. and M.F.M.Y.; formal analysis, M.F.M.Y. and H.A.A.; investigation, M.F.M.Y. and H.A.A.; data curation, B.H.H., M.F.M.Y. and H.A.A.; writing—original draft preparation, S.S.A.; writing—review and editing, J.P.G., B.H.H., M.F.M.Y. and H.A.A.; supervision, K.D.A.; project administration, K.D.A.; funding acquisition, K.D.A. All authors have read and agreed to the published version of the manuscript.

Funding: This research was funded by the Researchers Supporting Project number (RSPD2023R633), King Saud University, Riyadh, Saudi Arabia.

Data Availability Statement: The data reported in this study are available on reasonable request from the corresponding author.

Acknowledgments: This research project was funded by the Researchers Supporting Project number (RSPD2023R633), king Saud University, Riyadh, Saudi Arabia.

Conflicts of Interest: The authors declare no conflict of interest.

References

1. Rajendran, S.; Priya, A.K.; Senthil Kumar, P.; Hoang, T.K.A.; Sekar, K.; Chong, K.Y.; Khoo, K.S.; Ng, H.S.; Show, P.L. A critical and recent developments on adsorption technique for removal of heavy metals from wastewater—A review. *Chemosphere* **2022**, *303*, 135146. [CrossRef] [PubMed]
2. Liu, X.; Wang, Y.; Chang, J. A review on the incorporation and potential mechanism of heavy metals on the recovered struvite from wastewater. *Water Res.* **2021**, *207*, 117823. [CrossRef] [PubMed]
3. Xiang, H.; Min, X.; Tang, C.-J.; Sillanpää, M.; Zhao, F. Recent advances in membrane filtration for heavy metal removal from wastewater: A mini review. *J. Water Process Eng.* **2022**, *49*, 103023. [CrossRef]
4. Iqbal, M.O.; Yahya, E.B. In vivo assessment of reversing aminoglycoside antibiotics nephrotoxicity using *Jatropha mollissima* crude extract. *Tissue Cell* **2021**, *72*, 101525. [CrossRef] [PubMed]
5. Yusop, M.F.M.; Jaya, E.M.J.; Ahmad, M.A. Single-stage microwave assisted coconut shell based activated carbon for removal of Zn(II) ions from aqueous solution—Optimization and batch studies. *Arab. J. Chem.* **2022**, *15*, 104011. [CrossRef]
6. Mirzabeygi, M.; Abbasnia, A.; Yunesian, M.; Nodehi, R.N.; Yousefi, N.; Hadi, M.; Mahvi, A.H. Heavy metal contamination and health risk assessment in drinking water of Sistan and Baluchistan, Southeastern Iran. *Hum. Ecol. Risk Assess. Int. J.* **2017**, *23*, 1893–1905. [CrossRef]
7. Afroze, S.; Sen, T.K. A Review on Heavy Metal Ions and Dye Adsorption from Water by Agricultural Solid Waste Adsorbents. *Water Air Soil Pollut.* **2018**, *229*, 225. [CrossRef]
8. Zeng, G.; Wan, J.; Huang, D.; Hu, L.; Huang, C.; Cheng, M.; Xue, W.; Gong, X.; Wang, R.; Jiang, D. Precipitation, adsorption and rhizosphere effect: The mechanisms for Phosphate-induced Pb immobilization in soils—A review. *J. Hazard. Mater.* **2017**, *339*, 354–367. [CrossRef]

9. Rezania, S.; Mojiri, A.; Park, J.; Nawrot, N.; Wojciechowska, E.; Marraiki, N.; Zaghloul, N.S.S. Removal of lead ions from wastewater using lanthanum sulfide nanoparticle decorated over magnetic graphene oxide. *Environ. Res.* **2022**, *204*, 111959. [CrossRef]
10. Goswami, L.; Arul Manikandan, N.; Pakshirajan, K.; Pugazhenthi, G. Simultaneous heavy metal removal and anthracene biodegradation by the oleaginous bacteria *Rhodococcus opacus*. *3 Biotech* **2017**, *7*, 37. [CrossRef] [PubMed]
11. Du, J.; Zhou, A.; Lin, X.; Bu, Y. Adsorption mechanism of Pb^{2+} in montmorillonite nanopore under various temperatures and concentrations. *Environ. Res.* **2022**, *209*, 112817. [CrossRef] [PubMed]
12. Zhang, X.; Lin, Q.; Luo, S.; Ruan, K.; Peng, K. Preparation of novel oxidized mesoporous carbon with excellent adsorption performance for removal of malachite green and lead ion. *Appl. Surf. Sci.* **2018**, *442*, 322–331. [CrossRef]
13. Gupta, K.M.; Zhang, K.; Jiang, J. Efficient removal of Pb^{2+} from aqueous solution by an ionic covalent−organic framework: Molecular simulation study. *Ind. Eng. Chem. Res.* **2018**, *57*, 6477–6482. [CrossRef]
14. Xu, J.; Cao, Z.; Zhang, Y.; Yuan, Z.; Lou, Z.; Xu, X.; Wang, X. A review of functionalized carbon nanotubes and graphene for heavy metal adsorption from water: Preparation, application, and mechanism. *Chemosphere* **2018**, *195*, 351–364. [CrossRef]
15. Gherasim, C.V.; Křivčík, J.; Mikulášek, P. Investigation of batch electrodialysis process for removal of lead ions from aqueous solutions. *Chem. Eng. J.* **2014**, *256*, 324–334. [CrossRef]
16. Azamat, J.; Sardroodi, J.J.; Poursoltani, L.; Jahanshahi, D. Functionalized boron nitride nanosheet as a membrane for removal of Pb^{2+} and Cd^{2+} ions from aqueous solution. *J. Mol. Liq.* **2021**, *321*, 114920. [CrossRef]
17. Lystvan, K.; Listvan, V.; Shcherbak, N.; Kuchuk, M. Rhizoextraction potential of convolvulus tricolor hairy roots for Cr^{6+}, Ni^{2+}, and Pb^{2+} removal from aqueous solutions. *Appl. Biochem. Biotechnol.* **2021**, *193*, 1215–1230. [CrossRef]
18. Manfrin, J.; Gonçalves, A.C., Jr.; Schwantes, D.; Conradi, E., Jr.; Zimmermann, J.; Ziemer, G.L. Development of biochar and activated carbon from cigarettes wastes and their applications in Pb^{2+} adsorption. *J. Environ. Chem. Eng.* **2021**, *9*, 104980. [CrossRef]
19. Yusop, M.F.M.; Mohd Johan Jaya, E.; Mohd Din, A.T.; Bello, O.S.; Ahmad, M.A. Single-stage optimized microwave-induced activated carbon from coconut shell for cadmium adsorption. *Chem. Eng. Technol.* **2022**, *45*, 1943–1951. [CrossRef]
20. Kongsune, P.; Rattanapan, S.; Chanajaree, R. The removal of Pb^{2+} from aqueous solution using mangosteen peel activated carbon: Isotherm, kinetic, thermodynamic and binding energy calculation. *Groundw. Sustain. Dev.* **2021**, *12*, 100524. [CrossRef]
21. Yusop, M.F.M.; Ahmad, M.A.; Rosli, N.A.; Gonawan, F.N.; Abdullah, S.J. Scavenging malachite green dye from aqueous solution using durian peel based activated carbon. *Malays. J. Fundam. Appl. Sci.* **2021**, *17*, 95–103. [CrossRef]
22. Alharbi, H.A.; Hameed, B.H.; Alotaibi, K.D.; Al-Oud, S.S.; Al-Modaihsh, A.S. Recent methods in the production of activated carbon from date palm residues for the adsorption of textile dyes: A review. *Front. Environ. Sci.* **2022**, *10*, 1943–1951. [CrossRef]
23. Bello, O.S.; Ahmad, M.A. Removal of remazol brilliant violet-5R dye using periwinkle shells. *Chem. Ecol.* **2011**, *27*, 481–492. [CrossRef]
24. Quesada, H.B.; de Araújo, T.P.; Cusioli, L.F.; de Barros, M.A.S.D.; Gomes, R.G.; Bergamasco, R. Caffeine removal by chitosan/activated carbon composite beads: Adsorption in tap water and synthetic hospital wastewater. *Chem. Eng. Res. Des.* **2022**, *184*, 1–12. [CrossRef]
25. Aziz, A.; Khan, M.N.N.; Yusop, M.F.M.; Jaya, M.J.J.; Jaya, M.A.T.; Ahmad, M.A. Single-stage microwave-assisted coconut-shell-based activated carbon for removal of dichlorodiphenyltrichloroethane (DDT) from aqueous solution: Optimization and batch studies. *Int. J. Chem. Eng.* **2021**, *2021*, 9331386. [CrossRef]
26. Li, S.; Cho, M.-K.; Lee, K.; Deng, S.; Zhao, L.; Yuan, X.; Wang, J. Diamond in the rough: Polishing waste polyethylene terephthalate into activated carbon for CO_2 capture. *Sci. Total Environ.* **2022**, *834*, 155262. [CrossRef]
27. Mohamad Yusop, M.F.; Abdullah, A.Z.; Ahmad, M.A. Malachite green dye adsorption by jackfruit based activated carbon: Optimization, mass transfer simulation and surface area prediction. *Diam. Relat. Mater.* **2023**, *136*, 109991. [CrossRef]
28. Mbarki, F.; Selmi, T.; Kesraoui, A.; Seffen, M. Low-cost activated carbon preparation from Corn stigmata fibers chemically activated using H_3PO_4, $ZnCl_2$ and KOH: Study of methylene blue adsorption, stochastic isotherm and fractal kinetic. *Ind. Crops Prod.* **2022**, *178*, 114546. [CrossRef]
29. Ramutshatsha-Makhwedzha, D.; Mavhungu, A.; Moropeng, M.L.; Mbaya, R. Activated carbon derived from waste orange and lemon peels for the adsorption of methyl orange and methylene blue dyes from wastewater. *Heliyon* **2022**, *8*, e09930. [CrossRef]
30. Firdaus, M.Y.M.; Aziz, A.; Azmier Ahmad, M. Conversion of teak wood waste into microwave-irradiated activated carbon for cationic methylene blue dye removal: Optimization and batch studies. *Arab. J. Chem.* **2022**, *15*, 104081. [CrossRef]
31. Haghbin, M.R.; Niknam Shahrak, M. Process conditions optimization for the fabrication of highly porous activated carbon from date palm bark wastes for removing pollutants from water. *Powder Technol.* **2021**, *377*, 890–899. [CrossRef]
32. Ahmad, F.; Daud, W.M.A.W.; Ahmad, M.A.; Radzi, R. The effects of acid leaching on porosity and surface functional groups of cocoa (*Theobroma cacao*)-shell based activated carbon. *Chem. Eng. Res. Des.* **2013**, *91*, 1028–1038. [CrossRef]
33. Yusop, M.F.M.; Ahmad, M.A.; Rosli, N.A.; Manaf, M.E.A. Adsorption of cationic methylene blue dye using microwave-assisted activated carbon derived from acacia wood: Optimization and batch studies. *Arab. J. Chem.* **2021**, *14*, 103122. [CrossRef]
34. Lai, H.J. Adsorption of remazol brilliant violet 5R (RBV-5R) and remazol brilliant blue R (RBBR) from aqueous solution by using agriculture waste. *Trop. Aquat. Soil Pollut.* **2021**, *1*, 11–23. [CrossRef]
35. Bouchelkia, N.; Mouni, L.; Belkhiri, L.; Bouzaza, A.; Bollinger, J.-C.; Madani, K.; Dahmoune, F. Removal of lead(II) from water using activated carbon developed from jujube stones, a low-cost sorbent. *Sep. Sci. Technol.* **2016**, *51*, 1645–1653. [CrossRef]

36. Chedri Mammar, A.; Mouni, L.; Bollinger, J.-C.; Belkhiri, L.; Bouzaza, A.; Assadi, A.A.; Belkacemi, H. Modeling and optimization of process parameters in elucidating the adsorption mechanism of Gallic acid on activated carbon prepared from date stones. *Sep. Sci. Technol.* **2020**, *55*, 3113–3125. [CrossRef]
37. Mohamad Yusop, M.F.; Nasehir Khan, M.N.; Zakaria, R.; Abdullah, A.Z.; Ahmad, M.A. Mass transfer simulation on remazol brilliant blue R dye adsorption by optimized teak wood Based activated carbon. *Arab. J. Chem.* **2023**, *16*, 104780. [CrossRef]
38. Mohamad Yusop, M.F.; Tamar Jaya, M.A.; Idris, I.; Abdullah, A.Z.; Ahmad, M.A. Optimization and mass transfer simulation of remazol brilliant blue R dye adsorption onto meranti wood based activated carbon. *Arab. J. Chem.* **2023**, *16*, 104683. [CrossRef]
39. Al Harthi, S.; Mavazhe, A.; Al Mahroqi, H.; Khan, S.A. Quantification of phenolic compounds, evaluation of physicochemical properties and antioxidant activity of four date (*Phoenix dactylifera* L.) varieties of Oman. *J. Taibah Univ. Med. Sci.* **2015**, *10*, 346–352. [CrossRef]
40. Alotaibi, K.D.; Alharbi, H.A.; Yaish, M.W.; Ahmed, I.; Alharbi, S.A.; Alotaibi, F.; Kuzyakov, Y. Date palm cultivation: A review of soil and environmental conditions and future challenges. *Land Degrad. Dev.* **2023**, *34*, 2431–2444. [CrossRef]
41. Rambabu, K.; AlYammahi, J.; Bharath, G.; Thanigaivelan, A.; Sivarajasekar, N.; Banat, F. Nano-activated carbon derived from date palm coir waste for efficient sequestration of noxious 2,4-dichlorophenoxyacetic acid herbicide. *Chemosphere* **2021**, *282*, 131103. [CrossRef] [PubMed]
42. Alharbi, H.A.; Hameed, B.H.; Alotaibi, K.D.; Aloud, S.S.; Al-Modaihsh, A.S. Mesoporous Activated Carbon from Leaf Sheath Date Palm Fibers by Microwave-Assisted Phosphoric Acid Activation for Efficient Dye Adsorption. *ACS Omega* **2022**, *7*, 46079–46089. [CrossRef] [PubMed]
43. Zamouche, M.; Mouni, L.; Ayachi, A.; Merniz, I. Use of commercial activated carbon for the purification of synthetic water polluted by a pharmaceutical product. *Desalin. Water Treat.* **2019**, *172*, 86–95. [CrossRef]
44. Langmuir, I. The adsorption of gases on plane surfaces of glass, mica and platinum. *J. Am. Chem. Soc.* **1918**, *40*, 1361–1403. [CrossRef]
45. Freundlich, H.M.F. Over the adsorption in solution. *J. Phys. Chem.* **1906**, *57*, 385–471.
46. Parmanbek, N.; Sütekin, D.S.; Barsbay, M.; Mashentseva, A.A.; Zheltov, D.A.; Aimanova, N.A.; Jakupova, Z.Y.; Zdorovets, M.V. Hybrid PET track-etched membranes grafted by well-defined poly(2-(dimethylamino)ethyl methacrylate) brushes and loaded with silver nanoparticles for the removal of as(iii). *Polymers* **2022**, *14*, 4026. [CrossRef]
47. Marrakchi, F.; Hameed, B.H.; Bouaziz, M. Mesoporous and high-surface-area activated carbon from defatted olive cake by-products of olive mills for the adsorption kinetics and isotherm of methylene blue and acid blue 29. *J. Environ. Chem. Eng.* **2020**, *8*, 104199. [CrossRef]
48. Lagergren, S.K. About the theory of so-called adsorption of soluble substances. *Sven. Vetensk. Handingarl* **1898**, *24*, 1–39.
49. Ho, Y.S.; McKay, G. Sorption of dye from aqueous solution by peat. *Chem. Eng. J.* **1998**, *70*, 115–124. [CrossRef]
50. Lima, E.C.; Hosseini-Bandegharaei, A.; Moreno-Piraján, J.C.; Anastopoulos, I. A critical review of the estimation of the thermodynamic parameters on adsorption equilibria. Wrong use of equilibrium constant in the Van't Hoof equation for calculation of thermodynamic parameters of adsorption. *J. Mol. Liq.* **2019**, *273*, 425–434. [CrossRef]
51. Hijab, M.; Parthasarathy, P.; Mackey, H.R.; Al-Ansari, T.; McKay, G. Minimizing adsorbent requirements using multi-stage batch adsorption for malachite green removal using microwave date-stone activated carbons. *Chem. Eng. Process.—Process Intensif.* **2021**, *167*, 108318. [CrossRef]
52. Canales-Flores, R.A.; Prieto-García, F. Taguchi optimization for production of activated carbon from phosphoric acid impregnated agricultural waste by microwave heating for the removal of methylene blue. *Diam. Relat. Mater.* **2020**, *109*, 108027. [CrossRef]
53. Liu, H.; Liu, J.; Huang, H.; Evrendilek, F.; Wen, S.; Li, W. Optimizing bioenergy and by-product outputs from durian shell pyrolysis. *Renew. Energy* **2021**, *164*, 407–418. [CrossRef]
54. Martinez, C.L.M.; Rocha, E.P.A.; Carneiro, A.O.; Gomes, F.J.B.; Batalha, L.A.R.; Vakkilainen, E. Characterization of residual biomasses from the coffee production chain and assessment the potential for energy purposes. *Biomass Bioenergy* **2019**, *120*, 68–76. [CrossRef]
55. Tan, Y.L.; Abdullah, A.Z.; Hameed, B.H. Product distribution of the thermal and catalytic fast pyrolysis of karanja (Pongamia pinnata) fruit hulls over a reusable silica-alumina catalyst. *Fuel* **2019**, *245*, 89–95. [CrossRef]
56. Neme, I.; Gonfa, G.; Masi, C. Activated carbon from biomass precursors using phosphoric acid: A review. *Heliyon* **2022**, *8*, e11940. [CrossRef]
57. Maršálek, R.; Švidrnoch, M. The adsorption of amitriptyline and nortriptyline on activated carbon, diosmectite and titanium dioxide. *Environ. Chall.* **2020**, *1*, 100005. [CrossRef]
58. Joshi, N.C.; Rawat, B.S.; Kumar, P.; Kumar, N.; Upadhyay, S.; Chetana, S.; Gururani, P.; Kimothi, S. Sustainable synthetic approach and applications of ZnO/r-GO in the adsorption of toxic Pb^{2+} and Cr^{6+} ions. *Inorg. Chem. Commun.* **2022**, *145*, 110040. [CrossRef]
59. Liu, L.; Huang, Y.; Cao, J.; Hu, H.; Dong, L.; Zha, J.; Su, Y.; Ruan, R.; Tao, S. Qualitative and relative distribution of Pb^{2+} adsorption mechanisms by biochars produced from a fluidized bed pyrolysis system under mild air oxidization conditions. *J. Mol. Liq.* **2021**, *323*, 114600. [CrossRef]
60. Mashentseva, A.A.; Aimanova, N.A.; Parmanbek, N.; Temirgaziyev, B.S.; Barsbay, M.; Zdorovets, M.V. *Serratula coronata* L. Mediated synthesis of ZnO nanoparticles and their application for the removal of alizarin yellow R by photocatalytic degradation and adsorption. *Nanomaterials* **2022**, *12*, 3293. [CrossRef]

61. Saleh, T.A.; Adio, S.O.; Asif, M.; Dafalla, H. Statistical analysis of phenols adsorption on diethylenetriamine-modified activated carbon. *J. Clean. Prod.* **2018**, *182*, 960–968. [CrossRef]
62. Altynbaeva, L.S.; Mashentseva, A.A.; Aimanova, N.A.; Zheltov, D.A.; Shlimas, D.I.; Nurpeisova, D.T.; Barsbay, M.; Abuova, F.U.; Zdorovets, M.V. Eco-friendly electroless template synthesis of cu-based composite track-etched membranes for sorption removal of lead(II) ions. *Membranes* **2023**, *13*, 495. [CrossRef] [PubMed]
63. Sepehri, S.; Kanani, E.; Abdoli, S.; Rajput, V.D.; Minkina, T.; Asgari Lajayer, B. Pb(II) Removal from aqueous solutions by adsorption on stabilized zero-valent iron nanoparticles & mdash;a green approach. *Water* **2023**, *15*, 222.
64. Wang, Q.; Wang, Y.; Yang, Z.; Han, W.; Yuan, L.; Zhang, L.; Huang, X. Efficient removal of Pb(II) and Cd(II) from aqueous solutions by mango seed biosorbent. *Chem. Eng. J. Adv.* **2022**, *11*, 100295. [CrossRef]
65. Gusain, R.; Kumar, N.; Fosso-Kankeu, E.; Ray, S.S. Efficient removal of Pb(II) and Cd(II) from industrial mine water by a hierarchical MoS2/SH-MWCNT Nanocomposite. *ACS Omega* **2019**, *4*, 13922–13935. [CrossRef]
66. Khoso, W.A.; Haleem, N.; Baig, M.A.; Jamal, Y. Synthesis, characterization and heavy metal removal efficiency of nickel ferrite nanoparticles (NFN's). *Sci. Rep.* **2021**, *11*, 3790. [CrossRef]
67. Mashentseva, A.A.; Seitzhapar, N.; Barsbay, M.; Aimanova, N.A.; Alimkhanova, A.N.; Zheltov, D.A.; Zhumabayev, A.M.; Temirgaziev, B.S.; Almanov, A.A.; Sadyrbekov, D.T. Adsorption isotherms and kinetics for Pb(II) ion removal from aqueous solutions with biogenic metal oxide nanoparticles. *RSC Adv.* **2023**, *13*, 26839–26850. [CrossRef]
68. Vázquez-Sánchez, A.Y.; Lima, E.C.; Abatal, M.; Tariq, R.; Santiago, A.A.; Alfonso, I.; Aguilar, C.; Vazquez-Olmos, A.R. Biosorption of Pb(II) using natural and treated *Ardisia compressa* K. leaves: Simulation framework extended through the application of artificial neural network and genetic algorithm. *Molecules* **2023**, *28*, 6387. [CrossRef]
69. Nyirenda, J.; Kalaba, G.; Munyati, O. Synthesis and characterization of an activated carbon-supported silver-silica nanocomposite for adsorption of heavy metal ions from water. *Results Eng.* **2022**, *15*, 100553. [CrossRef]
70. Preeti; Banerjee, S.; Debnath, A.; Singh, V. Gum ghatti-alginate hybrid bead derived titania spheres for deep removal of toxic dye Remazol Brilliant Violet from aqueous solutions. *Environ. Nanotechnol. Monit. Manag.* **2021**, *15*, 100459. [CrossRef]